Bright and dark excitons in semiconductor carbon nanotubes: insights from electronic structure calculations

Svetlana Kilina,[a] Ekaterina Badaeva,[b] Andrei Piryatinski,[a] Sergei Tretiak,*[a] Avadh Saxena[a] and Alan R. Bishop[a]

Received 20th October 2008, Accepted 2nd February 2009
First published as an Advance Article on the web 23rd March 2009
DOI: 10.1039/b818473a

We review electronic structure calculations of finite-length semiconducting carbon nanotubes using time-dependent density functional theory (TD-DFT) and the time dependent Hartree–Fock (TD-HF) approach coupled with semi-empirical AM1 and ZINDO Hamiltonians. We specifically focus on the energy splitting, relative ordering, and localization properties of optically active (bright) and optically forbidden (dark) states from the lowest excitonic band of the nanotubes. These excitonic states are very important in competing radiative and non-radiative processes in these systems. Our analysis of excitonic transition density matrices demonstrates that pure DFT functionals overdelocalize excitons making an electron–hole pair unbound; consequently, excitonic features are not presented in this method. In contrast, the pure HF and AM1 calculations overbind excitons, inaccurately predicting the lowest energy state as a bright exciton. Changing the AM1 with the ZINDO Hamiltonian in TD-HF calculations predicts the bright exciton as the second state after the dark one. However, in contrast to AM1 calculations, the diameter dependence of the excitation energies obtained by ZINDO does not follow the experimental trends. Finally, the TD-DFT approach incorporating hybrid functionals with a moderate portion of the long-range HF exchange, such as B3LYP, has the most generality and predictive capacity providing a sufficiently accurate description of excitonic structure in finite-size nanotubes. These methods characterize four important lower exciton bands: the lowest state is dark, the upper band is bright, and the two other dark and nearly degenerate excitons lie in between. Although the calculated energy splittings between the lowest dark and the bright excitons are relatively large ($\sim$0.1 eV), the dense excitonic manifold below the bright exciton allows for fast non-radiative relaxation leading to the rapid population of the lowest dark exciton. This rationalizes the low luminescence efficiency in nanotubes.

1. Introduction

Carbon nanotubes are one of the most auspicious examples of quasi-one-dimensional nanoscale materials which promise fascinating applications ranging from nanoelectronics[1–7] and optoelectronics[8–11] to medical technologies.[12] However, in order to complete their proof-of-concept development stage, as well as to extensively integrate them into common experimental, medicinal and household usage, a detailed understanding and rational control of the electronic structure and the optical response of these materials is required. It is well recognized by now that the electron confinement along the circumference of the single-walled carbon nanotube (SWNT)

[a] *Theoretical Division, Center for Nonlinear Studies (CNLS), and Center for Integrated Nanotechnologies (CINT), Los Alamos National Laboratory, Los Alamos, NM 87545, USA. E-mail: serg@lanl.gov*
[b] *University of Washington, Seattle, WA 98195, USA*

Svetlana Kilina

Svetlana Kilina received her BSc and MSc degrees in physics from Belarus State University in 1996 and completed a PhD in physical chemistry at the University of Washington in 2007. Since 2008 she has been a postdoctoral fellow at Los Alamos National Laboratory. Her research is focused on photoinduced electron–phonon dynamics in nanoscale systems, such as quantum dots, carbon nanotubes, conjugated polymers, and DNA materials.

Ekaterina Badaeva

Ekaterina Badaeva received BSc and MSc degrees in materials science from Mendeleev's University of Chemical Technology, Russia, in 2003 and is currently pursuing PhD research in physical/theoretical chemistry at the University of Washington. Her research focus is the ground- and excited-state electronic structure of semiconductor quantum dots; electronic excitations in nanomaterials; nonlinear optical response of chromophores and dendrimers.

and its small dielectric constant lead to significant electron–hole binding energies and the formation of strongly bound excitons—strongly interacting electron–hole pairs—as the primary photoexcited species. Theoretical studies,[13–15] transient spectroscopy and nonlinear absorption experiments[16–18] have unambiguously proven that the lower energy optical excitations of SWNTs involve transitions to exciton states with large binding energies of 0.2–0.5 eV,[19–21] depending on the tube diameter and chirality.

In addition, complex Coulombic interactions drive the existence of optically inactive (dark) excitons energetically closer to each of the optically allowed (bright) excitons. In a single particle representation, the states at the edges of conduction (CB) and valence (VB) bands in SWNTs are doubly degenerate because of the cylindrical symmetry of the tube. For free electron–hole pairs, this leads to four distinct but degenerate interband transitions with different angular momenta.[22,23] However, the Coulombic interaction between a photoexcited electron and a hole lifts the degeneracy and introduces a complex structure of overlapping excitons, where only one is optically bright and the others are dark because of the difference in their parity.[24,25] Interactions with the environment, edge effects, defects and impurities in the tube lattice further split and mix energies of excitonic bands.[26,27] Mixing between different excitons, due to interactions and deviations from the ideal tube structure, makes some optically forbidden states weakly active (semi-dark), rather than being strictly dark.[28–32]

Indeed, the energy position of the dark and semi-dark excitons with respect to the bright ones strongly affects the photophysical properties of SWNTs. Thus, recent theoretical studies[23–25,33,34] explain the typical low photoluminescence (PL) quantum yield in SWNTs by the possible involvement of a dark excitonic state below the first optically allowed exciton (E_{11}), trapping much of the exciton population. The experimental evidence for the existence of the lowest energy

Andrei Piryatinski

Andrei Piryatinski is a member of technical staff in the Theoretical Division at Los Alamos National Laboratory. He received his MS degree in theoretical physics from Kiev State University, Ukraine, and a PhD degree in Physics from The University of Toledo, USA. His research is focused on theoretical studies of ultrafast carrier dynamics and photoinduced electronic and vibration processes on nanometer length scale as well as theoretical, non-linear multidimensional spectroscopy.

Sergei Tretiak

Sergei Tretiak received his MSc degree from Moscow Institute of Physics and Technology, Russia, and his PhD degree from the University of Rochester. He is currently part of the DOE funded Center for Integrated Nanotechnologies (CINT) at Los Alamos National Laboratory. His research interests include nonlinear optical response of organic chromophores; molecular dynamics of the excited states; collective electronic excitations and optical response of conjugated polymers, carbon nanotubes, and semiconductor nanoparticles; time-dependent density functional theory and semi-empirical methods; charge and energy transfer in biological and artificial antenna complexes.

Avadh Saxena

Avadh Saxena obtained a PhD in physics from Temple University and is currently group leader of the Physics of Condensed Matter and Complex Systems group at Los Alamos National Laboratory, USA. His main research interests include optical, electronic, and vibrational properties of functional materials, device physics, phase transitions, soft condensed matter and nonlinear phenomena. He holds adjunct professor positions at the University of Barcelona and the University of Arizona.

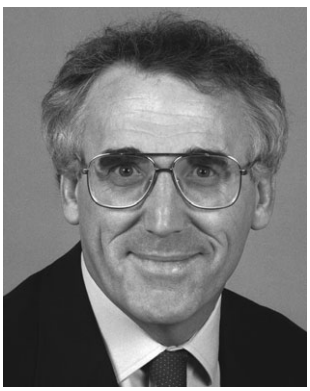

Alan Bishop

Alan Bishop earned a PhD in theoretical physics at the University of Cambridge, England. Since 1979, he has worked at Los Alamos National Laboratory, USA, where he is now Associate Director for Theory, Simulation, and Computation. Alan is a Fellow of the American Physical Society, Fellow of the American Association for the Advancement of Science, a recipient of the Department of Energy's E. O. Lawrence Award, a Humboldt Senior Fellow and a Laboratory Fellow. His research interests include physics of solitons, quantum complexity, structural and magnetic transitions, collective excitations in low-dimensional materials and materials with strong spin-charge-lattice coupling.

dark exciton has been obtained through magnetic brightening of SWNTs.[30,35] Time-resolved spectroscopy reveals multi-exponential behavior of the radiative photoluminescence (PL) decay at room[36] and low[28,37] temperatures, demonstrating at least two different characteristic decay times.[38] The first, fast, component can be associated with the rapid decay of the bright exciton to the lower-lying dark state. The long time dynamics are most readily accounted for by the trapping of a dark exciton that does not have a radiative recombination path.[36]

Although both experimental and theoretical results conclude that the lowest energy exciton in SWNTs is the dark one, the relative ordering of other optically inactive excitonic states with respect to the bright one and their role in photophysical processes in SWNTs is still unclear. For example, *ab initio* calculations of a few narrow tubes within the Bethe–Salpeter scheme[25] show that the two remaining dark states from the four-fold first band are degenerate and lie slightly above the bright exciton. Tight binding modeling, including electron–hole interactions *via* the Bethe–Salpeter equation,[23] also provides a similar energy band structure for the four lowest excitons. However, for long but finite-size tubes, calculations based on the semi-empirical Pariser–Parr–Pople (PPP) Hamiltonian[24,33] predict two degenerate dark states and one weakly allowed state in between the bright exciton and the lowest dark one. In addition, the splitting between the lowest dark and the bright excitons predicted by this semi-empirical model is significantly larger than those derived from the *ab initio* calculations.[25,34] Other semi-empirical calculations based on the time-dependent Hartree–Fock (TD-HF) approach combined with an Austin model 1 (AM1) Hamiltonian predict the bright exciton as the lowest energy state,[39] while the same method coupled with Zerner's intermediate neglect of differential overlap (ZINDO) Hamiltonian gives the bright exciton as the second state after the dark one and the two remaining states as semi-dark excitons lying above the bright state.[40] Finally, our previous first principle calculations based on the time-dependent density functional theory (TD-DFT), predict three nominally dark exciton bands below the bright exciton.[28]

It is quite remarkable that each of the suggested electronic structures for the first four-fold excitonic band (*i.e.* two dark or semi-dark states lying above or below the bright exciton) could be used as a reasonable model to describe the experimentally detected PL rates in SWNTs. For example, a two level model—the dark state followed by a bright one—was used to explain the transient absorption kinetics in (11,0) nanotubes.[37,41] However, the calculated relative positions of the three lowest energy dark bands with respect to the bright exciton are in good agreement with fluorescence spectra as a function of temperature, and successfully explain the dual emission features observed in (7,5) and (7,6) tube samples.[28] Thus, while qualitatively consistent, the precise ordering of bright and dark excitons, their energy splitting values and the dependence on the tube geometry are highly method-dependent and still under debate.

In the present work, we further explore low-energy dark and bright excitons, their ordering, sensitive energetics, optical activity and the dependence of the splitting between these states on the tube chirality and diameter by applying a TD-DFT methodology. It is important to note that TD-DFT is currently a mainstream approach and a method of choice for quantitative modeling of optical response in large molecular systems. However, this method was not broadly applied to SWNTs. Previously, we used TD-DFT to study electronic properties and energetics of singlet[28] and triplet[42] states in (7,5) and (7,6) tubes. Here we extend our studies to ten finite-size SWNTs with diameters ranging from 0.5–1.5 nm. We specifically explore the effect of different DFT functionals on the splitting between dark and bright singlet states and compare these results with TD-HF calculations based on semi-empirical Hamiltonians.

The outline of the paper is as follows. In section 2 we briefly define the methods that we use and sketch computational details. In section 3 we first compare the absorption spectra of SWNTs calculated with different DFT functionals. Then we report the localization properties of lower energy excitons based on the analysis of transition density matrices and identify four main excitonic bands, including optically dark and bright states. Also, the effect of the nanotube length and the changes in exciton energies and localization properties imposed by a different portion of the HF exchange in the functional are discussed in detail. Next, the dependence of the energy splitting between the lowest dark excitons and the bright excitons on the tube diameter is obtained and analyzed. The TD-DFT results are also compared with semi-empirical methods in subsection 3.2. Finally, concluding remarks are given in section 4.

2. Methods and computational details

2.1 Description of SWNTs studied

Each of the ten SWNTs we investigate here has a length of 8–12 nm and comprises several repeat units (see Table 1). Such a length is significantly larger than the tube diameter and characteristic exciton sizes,[39,43] and, therefore, is expected to reproduce the basic properties of longer SWNTs and to be at least qualitatively consistent with the infinite-size limit. Calculations of conjugated oligomers provide a standard example of such an approach.[44–46] On the other hand, the finite length of SWNTs introduces some extrinsic factors to the simulated systems. In contrast to the ideal nanotube systems typically considered in theory, actual SWNT samples can have inhomogeneity in the length (*i.e.*, some species have much smaller length compared to the averaged tube length), inhomogeneity of the local dielectric environment, defects, and intertube interactions. Indeed, all these extrinsic features affect electronic structure, exciton localization properties and the overall optical response of the system.

As for realistic tube lengths, SWNTs used in experiments typically have lengths of hundreds of micrometers. However, sample preparation such as sonication might lead to multiple nanotube breakages[47] and significant reduction of the average nanotube length down to 10–15 nm.[48] Thus, in experimental samples, tubes with small length, such as we consider here, can also be present. Since our tubes have a finite length, we cap unsaturated chemical bonds at the open tube ends with

Table 1 Optimal AM1 geometrical parameters (the diameter (d), the length (L), and the number of repeat unit cells), state number and the energy (E_B, eV) of the first bright exciton (B-state), and the splitting between the bright and dark state energies (δ_{B-D}, eV) calculated with different methods in the ten SWNTs studied

		SWNT										
Method	Parameter	(6,2)	(8,0)	(6,5)	(6,5)	(9,1)	(7,5)	(11,0)	(7,6)	(9,4)	(8,6)	(10,5)
	d/Å	5.65	6.26	7.47	7.47	7.50	8.17	8.61	8.85	9.03	9.52	10.39
	L/nm	10.7	11.1	8.2	11.8	11.9	9.0	8.8	9.7	9.9	10.0	10.8
	units	7	25	2	3	3	2	21	2	2	4	9
TD-PBE	B-state	6	10	5	6	6	6	4	4	4	4	6
	E_B	1.30	1.34	1.20	1.13	1.16	1.09	1.04	1.01	0.85	0.86	0.89
	δ_{B-D}	0.07	0.09	0.06	0.04	0.03	0.07	0.03	0.04	0.05	0.02	0.05
TD-B3LYP	B-state	7	12	7	7	8	7	7	7	14	7	7
	E_B	1.77	1.84	1.61	1.54	1.56	1.48	1.43	1.39	1.39	1.31	1.23
	δ_{B-D}	0.10	0.10	0.13	0.08	0.08	0.10	0.11	0.11	0.14	0.11	0.10
TD-BHand HLYP	B-state	5	4	5	5	5	5	5	5	9	5	5
	E_B	2.26	2.26	2.03	1.95	1.96	1.87	1.80	1.77	1.75	1.64	1.57
	δ_{B-D}	0.10	0.08	0.13	0.09	0.08	0.11	0.10	0.11	0.13	0.07	0.09
AM1	B-state	1	1	1	1	1	1	1	1	1	1	1
	E_B	1.23	1.24	1.09	1.05	1.15	1.03	1.05	0.97	0.98	0.95	0.94
ZINDO	B-state	22	6	2	2	2	2	2	2	2	2	2
	E_B	1.76	1.25	1.45	1.42	1.18	1.29	1.14	1.31	1.13	1.18	1.09
	δ_{B-D}	0.13	0.03	0.02	0.004	0.05	0.03	0.03	0.02	0.02	0.004	0.02
Exp.[57]	E_{11}	1.39	1.60	1.27	—	1.36	1.21	1.19	1.11	1.13	1.06	0.99

hydrogen atoms as described in detail in ref. 39. Such capping allows us to eliminate mid-gap states caused by dangling bonds and opens a band gap in finite-size SWNTs.

2.2 Geometry optimization

Optimal geometries of all tubes are obtained using the semi-empirical AM1 Hamiltonian,[49] as implemented in the MOPAC-2002 code.[50] This method works very well for geometry optimizations in a broad variety of π-conjugated molecules. In SWNTs, due to their rigid geometry, the electronic structure is expected to be weakly dependent on the optimized geometries. Our previous calculations of a (7,6) tube[42] show that optimizations conducted with other methods lead to small ($\sim$40 meV) and uniform red (DFT geometries) or blue (HF geometries) shifts of excitation energies, compared to AM1 geometries. We note that AM1 reproduces the curvature mediated σ- and π-interactions and the relevant vibrational effects well enough both in the ground and excited state dynamics of SWNTs, which have previously explained experimental findings.[18,51,52] Taking into account the reduced computational cost in addition to all other benefits of this method, the AM1 approach is chosen for geometry optimizations of the SWNTs studied here.

2.3 TD-DFT excited state calculations

The AM1-optimized geometries provide input structures for further excited-state calculations performed by TD-DFT using the GAUSSIAN03 package.[53] The STO-3G basis set is employed to calculate energies and transition dipole moments of the lowest 15–20 singlet excitations in each SWNT and model their absorption spectra. We previously found[42] that increasing the basis set to 3-21G and 6-31G uniformly shifts excitation energies to the red by $\sim$0.15 eV at most, while further increase of the basis to 6-31G* has a negligible effect on the excitation energies. Importantly, all basis sets provide electronic state structures which are qualitatively the same. Therefore, we conclude that the STO-3G level is sufficient to present a useful qualitative picture.

The choice of the density functional is expected to be much more critical in order to accurately account for excited state electronic correlations and reproduce the excitonic structure in SWNTs. It is well known that the hybrid TD-DFT technique can account for excitonic phenomena due to the presence of a fraction of the long-range HF exchange. The excitonic size and its localization properties show strong dependence on the amount of the HF exchange. For example, in conjugated polymers, at 0% of HF exchange (LDA and GGA limits), there are no excitonic effects at all. In contrast, 100% of exchange (HF limit) would overbind the excitons.[54] The right amount of orbital exchange is thus essential to capture excitonic effects and obtain correct electronic structure in π-systems, including SWNTs. 20% (B3LYP) of orbital exchange typically produces the most accurate results for most organic molecules and, therefore, is expected to simulate an accurate excitonic structure in SWNTs. The performance of TD-PBE and TD-BLYP (GGA functionals), TD-B3LYP, TD-BHandHLYP (50% of HF exchange) and TD-HF functionals for the first band singlet manifold in SWNTs is carefully studied in this work (see Table 1).

To investigate localization/delocalization properties of excitons, we further use a two-dimensional real-space analysis of transition density matrices, representing the electronic transition between the ground state and an optically excited state.[39,46] Photoexcitation creates an electron–hole pair or an exciton by transforming an electron from an occupied valence band to an

unoccupied conduction band. Each element of the transition density matrix reflects the dynamics of this exciton projected on a pair of atomic orbitals (AO) given by its indices. Contour plots of these matrices thus show accompanying motions of optically induced charges and electronic coherences. Two characteristic lengths are relevant in these plots: the diagonal direction of the non-zero matrix elements reflects the degree of localization of the optical excitation, *i.e.*, the position of the center of mass of the exciton. The largest off-diagonal extent of the non-zero matrix area—coherence length, L_C—measures the maximal distance between the electron and hole (the exciton size). The larger the exciton size, L_C, the less binding between an electron–hole pair is expected. Both cross-sections of transition density matrices are shown below in Fig. 2.

2.4 Semi-empirical calculations of excited states

In addition to TD-DFT calculations, we also calculate vertical transition frequencies from the ground state to the singlet excited states, their oscillator strengths and transition density matrices using the semi-empirical approach based on the collective electronic oscillator (CEO) procedure. The CEO approach, described in detail elsewhere,[39,46] involves the TD-HF formalism combined with semiempirical Hamiltonians. Here, we use both AM1 and ZINDO Hamiltonians. The TD-HF approximation coupled with semi-empirical Hamiltonians directly addresses essential electronic correlations and excitonic effects, while permitting calculations of hundreds of molecular excited states in very large systems (here, up to 1300 atoms in size) with only moderate numerical expense. This methodology has been successfully applied to simulations of optical responses in a variety of conjugated molecular materials.[55,56] Recently, we used this technique to investigate a number of excited-state phenomena in SWNTs, including anharmonic coherent phonon dynamics,[18] quantification of exciton-phonon coupling constants,[52] effects of Peierls distortion and exciton self-trapping,[39,43] characterization of high-energy excitonic transitions (E_{33} and E_{44})[51] and analysis of parallel (E_{11}) and cross-polarized (E_{12} and E_{21}) excitons.[40] We carefully examine the dependence of the excitonic energies, specifically the bright–dark exciton splitting, on the parameters characterizing the softness of the π- and σ-bonds by changing the values of these parameters in the ZINDO Hamiltonian. These results are compared to AM1 and TD-DFT calculations, and to available experimental data (Table 1).

3. Results and discussion

3.1 Variation of excitonic structure and optical spectra with density functional

Fig. 1 compares the spectra of all possible transitions, including dark and optically active transitions (absorption spectra) calculated with different DFT functionals for the (6,5) tube. As expected, pure GGA functionals, BLYP and PBE, result in red shifted excitation energies of both optically forbidden and allowed transitions. In contrast, increase in the portion of the HF exchange leads to a significant blue shift. For the considered energy range of about 0.6 eV, all functionals provide one state that collects most of the oscillator strength from its parent band. Thus, this state contributes most to the first distinct peak in the SWNT's linear absorption spectra, which is commonly associated with the E_{11} transition. The second small peak is roughly 0.2–0.4 eV away from the first one. This peak is formed from the states from the first excitonic band with a higher kinetic energy. The small oscillator strength of such states arises from the exciton scattering on the tube ends leading to the mixing of these states with the bright exciton. Increasing the portion of the HF exchange in the functional causes this second small peak to be consistently blue shifted and its relative intensity decreases with respect to the large first peak. Consequently, the presence of the long-range orbital exchange in the functional, which results in more localized excitons,[54] leads to a significant reduction of the second peak intensity in the HF-limit.

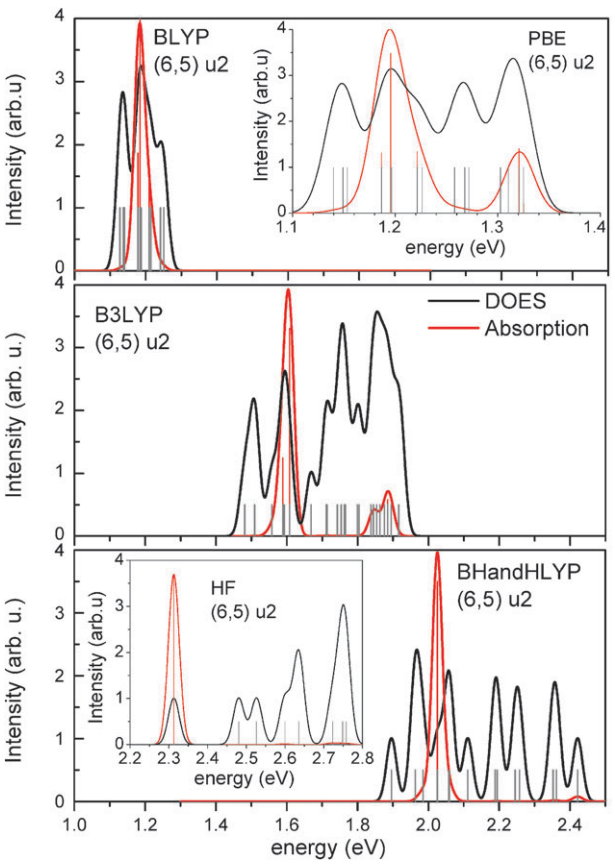

Fig. 1 Comparison of the density of all possible transitions and optically allowed transitions related to the E_{11} manifold in a (6,5) nanotube of 8 nm length calculated with the TD-DFT approach. The black solid line shows the density of all possible, including optically forbidden, transitions through the band gap. This density is normalized so that it shows the number of transitions in the defined energy range. Red solid line shows linear absorption spectra. All spectra are broadened with a Gaussian width of 0.01 eV. Vertical gray lines represent all transitions through the band gap, while the red vertical lines correspond to the oscillator strengths of these transitions. Top panel (with inset) shows GGA results, whereas middle and bottom (with inset) panels display hybrid functionals data with small and large fractions of orbital exchange, respectively.

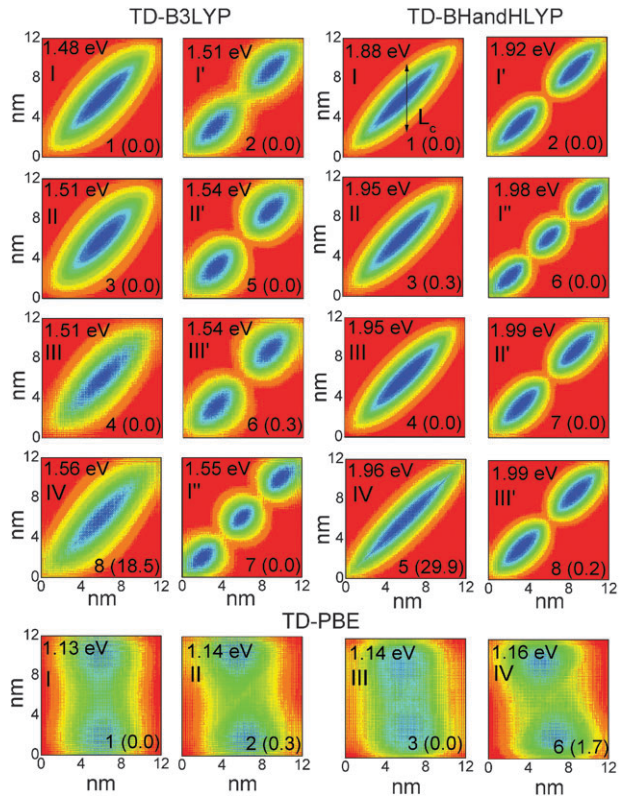

Fig. 2 Excitonic transition density matrices of a (9,1) tube calculated using TD-DFT and different functionals. The first eight excitons are presented by two-dimensional contour plots as a function of the electron (vertical axis, nanometers) and hole (horizontal axis, nanometers) coordinates along the tube axis. The amplitudes scale from red (0) to violet (1) through the natural rainbow color sequence. Excitons are labeled according to their order number with respect to the ground state (the right corner of each plot). The transition energy (in eV) and the oscillator strength (in parenthesis) are also shown for each excitonic state. The lowest state in each excitonic band I, II, III, and IV has no diagonal nodes (the first and third columns, and the lowest row). The diagonal direction reflects the distribution of the excitonic wavefunctions along the tube axis. The off-diagonal direction (L_c) characterizes the coherence size of an exciton. For the PBE functional, the states are completely delocalized, so that there is no excitonic effect at all. With increase of the HF portion in the functional, the excitons become more localized, demonstrating a smaller L_c for the case of BHandHLYP (50% of HF exchange), compared to B3LYP (20% of HF exchange).

For all considered DFT functionals, the presence of several dark states below the bright exciton is clearly seen in Fig. 1. Thus, the bright exciton is the fifth state from the lowest state predicted by TD-BLYP, TD-PBE, and BHandHLYP calculations of the (6,5) tube, while it is the seventh state in TD-B3LYP approach. In contrast, HF provides the lowest energy state as the bright one. As expected, based on the results obtained for conjugated polymers,[54] the TD-HF not only significantly overestimates the excitation energies, but also overbinds excitons and unrealistically lowers the energy of the bright exciton with respect to other dark states. A similar trend in the bright–dark state ordering and its dependence on the functional is observed for all other tubes, as presented in Table 1. The main conclusion drawn from Fig. 1 and Table 1 is that calculations involving the pure and hybrid DFT functionals result in several optically forbidden (or nearly forbidden) exciton states positioned slightly below ($\sim$0.1 eV) the bright state in all the considered SWNTs. While the splitting between the bright and the lowest dark state stays nearly the same for hybrid functionals, the relative numbering of the bright exciton, with respect to the lowest dark one, varies.

To explain the observed difference in the ordering of the bright exciton and its dependence on the functional, we recall that each exciton forms a band owing to the periodicity of the wave function along the tube axis. Stated differently, in quasi-one-dimensional structures, delocalized excited states can be considered as standing waves. Then, the number of nodes in their transition charge density is related to the exciton momenta, k.[55] Consequently, the zero-node state is associated with the $k = 0$ momentum exciton in the infinite-size limit. States having one or more nodes in their transition densities belong to the same band as the respective zero-node exciton but will have higher momenta ($k \geq 1$) in the infinite-size limit. Note that, owing to their finite-length, quantum confinement is introduced in the SWNTs considered and, thus, their electronic structure has a ladder of levels for each exciton band rather than a continuous band. The density of states in each exciton band will increase as the SWNT length approaches infinity under ideal conditions.

The transition density matrices for each state, plotted in a real-space representation in Fig. 2, demonstrate a characteristic standing wave structure of low energy excitons and enable us to assign each band. For example, for TD-B3LYP calculations, four bands are seen, with their lowest states (zero-node excitons) being numbered 1, 3, 4, and 8 in Fig. 2, first column. The standing waves for the next states in each band have one node, for example, numbers 2, 5, and 6, second column in Fig. 2. We label each exciton band I, II, III, and IV, as indicated in Fig. 2, and the sub-band states with one or more nodes are marked as I′, I″, II′, III′, and so on. Independent of the functional used, excitons II and III (zero-node states) are always dark or semi-dark and nearly degenerate. These states have energy lower than that of the bright exciton IV, but higher than the energy of the dark exciton I for all the tubes considered.

In contrast, the relative energy position of the sub-band states having node structure is very sensitive to the portion of the HF-exchange changes in the functional. Thus, for BHandHLYP calculations, only the sub-band state I′ (with one node) has energy smaller than the bright exciton IV, so that the bright exciton is the fifth state from the ground state for all tubes (see Table 1). However, in the case of the B3LYP functional, not only sub-band state I′ but also sub-band II′, III′, and even I″ (with two nodes) have lower energies than the bright exciton IV. Therefore, B3LYP calculations provide the bright exciton as the eighth state from the ground state in the (9,1) tube. For most tubes, however, the I″ state is slightly higher in energy than the IV exciton. Therefore, the bright exciton is the seventh state in B3LYP calculations for most nanotubes (Table 1). For the (8,0) and the (9,4) tubes, even more sub-band excitons with higher kinetic energies are introduced in between the I and IV zero-node excitons. For

PBE calculations, a similar uncertainty, associated with the tube chirality, in predicting sub-band energies is reflected in the numbering of the bright state with respect to the ground state (Table 1).

In summary, all functionals result in three dark exciton bands below the fourth bright exciton. Importantly, the energy splitting of zero-node dark and bright excitons remains almost independent of the functional. However, a decrease in the portion of the HF exchange in the functional affects the relative energy ordering of the sub-band states (with the node structure), showing its dependence on the tube chirality. Such sensitivity of the sub-band excitonic energies with respect to the tube chirality in the case of the functionals with a small or zero portion of the HF exchange can be explained by an increase in the delocalized character of excitons with a decrease in the long-range exchange portion in the functional. For the B3LYP functional, in fact, this delocalization leads to a smaller energy splitting ($\sim$0.03 eV) between states inside the band compared to those calculated by BHandHLYP ($\sim$0.04 eV). Therefore, TD-B3LYP calculations predict a larger number of sub-band states in between the lowest dark exciton I and the bright exciton IV than the TD-BHandHLYP approach.

The exciton delocalization trend in the limit of pure DFT functionals is clearly reflected in the transition density distribution presented in Fig. 2 (lowest row). All transition densities obtained by the PBE model represent completely delocalized excitons. For this calculation, the coherence size of excitons (L_c)—the off-diagonal cross-section of the transition density matrix—is undefined approaching infinity. Consequently, the PBE functional does not provide excitonic features at all, leading to over-delocalized and non-bound electron–hole states in SWNTs. Analogous results have also been obtained for excitons in conjugated polymers.[54] Thus, we conclude that pure DFT functionals cannot be applied for calculations of excitonic properties of SWNTs. In contrast, all hybrid functionals recover bound excitonic states with significant degrees of spatial localization, Fig. 2 (top panels). Comparison of exciton sizes calculated using B3LYP and BHandHLYP functionals, shows a much smaller L_c predicted by the BHandHLYP model. Thus, exciton localization increases with an increase of the HF-exchange. Indeed, excitons with a nodal structure (*i.e.*, with higher kinetic energy) have a more delocalized character compared to the zero-node excitons, specifically near the tube edges. Therefore, such states interact more strongly with tube ends. As a result of this interaction, the tube geometry, including chirality, capping and length, should more significantly affect sub-band states than zero-node excitons.

Note that because of the stronger delocalization, specifically for PBE and B3LYP calculations, excitons with one or more nodes can easily mix with the other excitons, including the bright one, gaining some oscillator strength. For example, either sub-band exciton III′ or II′ is usually semi-dark for all tubes calculated by TD-B3LYP. As can be seen in the absorption spectra of the tube (6,5), Fig. 1, in the case of the functionals with a zero (PBE and BLYP) and small (B3LYP) portion of the HF exchange, the brightest state is accompanied by nearly isoenergetic semi-dark sub-band states, *e.g.*, states 4 and 6 in PBE calculations and state 5 in B3LYP calculations. The oscillator strength of these sub-band states vanishes in the spectra calculated using functionals with a higher percentage of the HF exchange (BHandHLYP and HF limits). Similar to excitons in the tube (9,1) shown in Fig. 2, the strongly delocalized character of the excitonic transition densities of the tube (6,5) obtained with GGA functionals leads to a substantial mixing between neighboring sub-band states. This mixing rationalizes the appearance of weakly optically allowed transitions close in energy to the brightest exciton in the spectra obtained by TD-GGA simulations, Fig. 1. Such trends in optical signatures as a function of the tube length may be detected in future spectroscopic measurements of finite size SWNTs or highly disordered samples.[47,48]

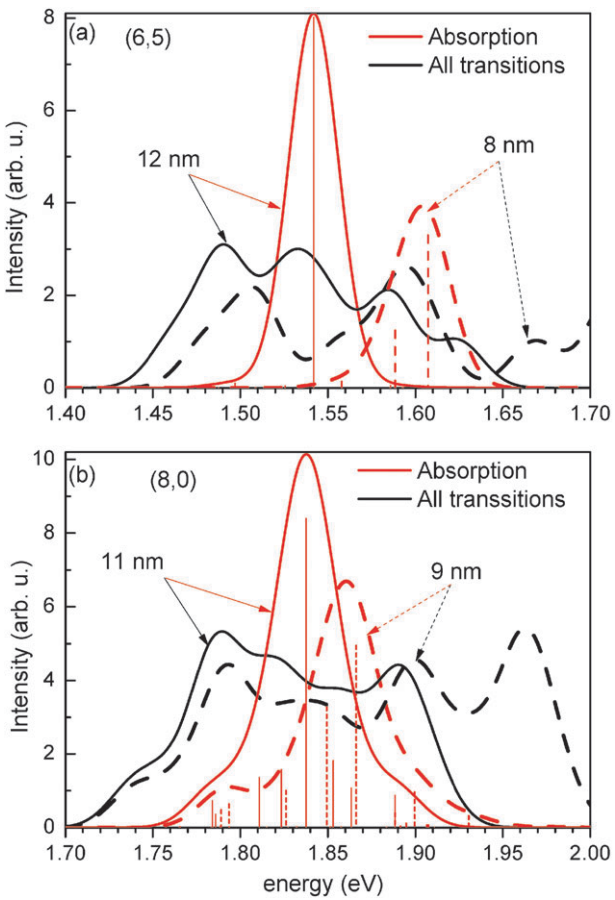

Fig. 3 Effect of the tube length on optically dark and bright states. The density of all possible transitions through the band gap (black lines) and absorption spectra (red lines) of (6,5) (a) and (8,0) (b) SWNTs of different lengths calculated with the TD-B3LYP model. Dashed lines correspond to spectra of shorter tubes, while solid lines show the spectra of longer tubes. The red vertical lines represent the oscillator strengths of optical transitions. The increase in the tube length leads to the red shift of transition energies. This shift is more pronounced for the first optically allowed transitions compared to the lowest-energy dark transitions. In the longer tubes, only one transition dominates the first absorption peak, while several transitions significantly contribute to the first absorption peak of shorter tubes, resulting in larger broadening and a complicated structure of spectra for short tube segments.

Increasing the tube length also leads to a weakening of the oscillator strength of such sub-band excitons. As can be seen in Fig. 3, for longer tubes calculated with the TD-B3LYP model, only one transition dominates the first absorption peak. For the shorter tubes, several other transitions significantly contribute to the first absorption peak, resulting in a larger broadening and more complicated structures of the absorption spectra of tubes with length <10 nm. When the length of the tube is much larger than the exciton size (0.3–0.5 nm),[39] interactions and mixing between different excitons are hindered, since excitons are more localized and not notably affected by the tube ends. Therefore, the main contribution to the absorption peak comes from only one exciton, namely IV, that is strongly optically allowed. In addition, increasing the tube length leads to a red shift of transition energies. Interestingly, this shift is more pronounced for the first optically allowed transitions compared to the lowest dark transitions. Consequently, the splitting between dark and bright excitons is smaller in longer nanotubes. It should be noted that TD-DFT calculations are relatively expensive, even when combined with a small basis set such as STO-3G. Therefore, we are limited to explore the whole range of possible lengths of tubes with this method. Nonetheless, our results obtained for several tube lengths (8, 9, 10, 11 and 12 nm) allow us to conclude that the qualitative structure of the optical spectra changes insignificantly with the length if the tubes are longer than 10 nm.

The dependence of the energies of the lowest dark I and bright IV excitons on the tube diameter, presented in Fig. 4, demonstrates good qualitative agreement with experimental data[57] for both TD-B3LYP and TD-BHandHLYP simulations. However, both functionals overestimate the exciton energies (by $\sim$0.3 eV, B3LYP, and $\sim$0.7 eV, BHandHLYP) compared to the experimental E_{11} transitions. This discrepancy can be explained by two reasons. The first one deals with the small basis set, STO-3G, used in our calculations. It was shown previously[42] that increasing the basis set to 6-31G would decrease transition energies by about 0.15 eV. Secondly, the finite length of the tubes considered further contributes to the blue shift of excitonic energies compared to the infinite-length limit in real SWNTs samples. Taking these reasons into account, we conclude that the TD-B3LYP model is sufficient for a reasonable quantitative picture of electronic excitations and, in particular, the energy splitting between bright and dark excitons in SWNTs. As was mentioned above, the splitting between the lowest dark and bright excitons is almost independent of the portion of the HF exchange in the functional. This splitting also shows a weak dependence on the tube chirality, Table 1. Roughly, the averaged bright–dark exciton splitting is about 0.1 eV. This value is much larger than the calculated splitting of 0.03 eV in the infinite-length tubes,[25,34] but very close to the results obtained for long finite tubes with the semi-empirical PPP model.[24,33]

It is important to note that in both *ab-initio*[25,34] and the effective-mass[23] calculations within the Bethe–Salpeter scheme of infinite tubes, the lowest dark exciton is followed by the bright one and then two dark, degenerate states lie above the bright exciton. In contrast, the semi-empirical modeling of long finite tubes[24,33] predicts doubly degenerate dark excitons to be in between the lowest dark exciton and the bright one,

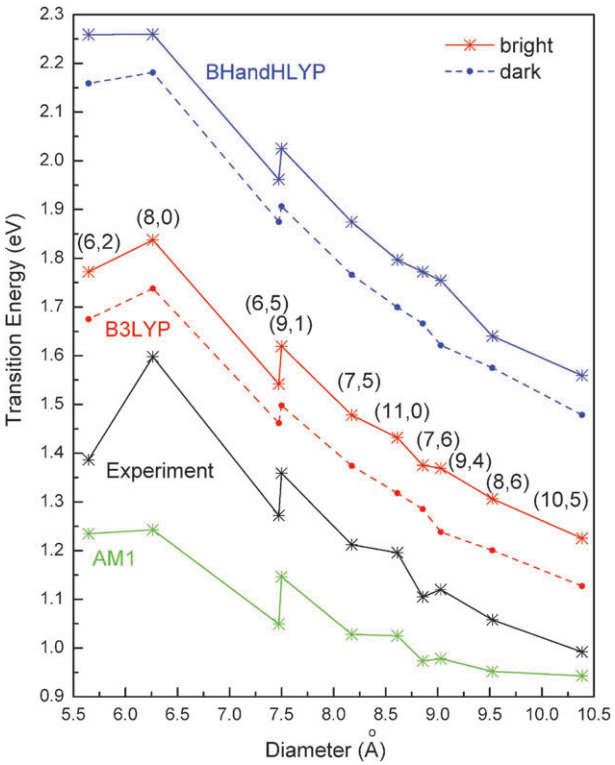

Fig. 4 Dependence of bright and dark excitonic energies on the tube diameter. Circles and dashed lines correspond to energies of the first dark excitons and stars and solid lines correspond to energies of the first bright excitons in different tubes calculated using TD-BHandHLYP, TD-B3LYP, and TD-HF-AM1 methods. The black line represents respective experimental data.[57] TD-B3LYP results demonstrate the best agreement with the experiment. Use of a small basis set and confinement effects due to the relatively small lengths (10–12 nm) of the tubes results in slightly larger energies of bright excitons obtained from TD-B3LYP calculations compared to the experimental values.

which is in agreement with our TD-DFT results. It was shown[24,33] that increase of the tube length from 10 to 40 nm decreases the energy of the dark-bright splitting by nearly half, while the relative ordering of the four lowest excitons remains unchanged. The lowering of doubly degenerate dark excitonic states with respect to the bright one may be related to the specific computational methodologies applied to the infinite-size tubes and finite clusters. Since there are no direct experimental data on the relative ordering of these optically inactive excitonic states with respect to the bright ones, conclusions on the reliability of either of the methods discussed are currently hindered.

3.2 Energies of bright and dark excitons in semi-empirical calculations

For comparison, the energy of the bright exciton calculated by TD-HF based on the semi-empirical AM1 Hamiltonian is also presented in Fig. 1, demonstrating a red shift of about 0.2 eV with respect to the experimental values of the first bright transition E_{11}. Similar to the TD-HF based on an *ab initio* Hamiltonian (see Fig. 1), AM1 calculations predict the lowest energy state as the bright exciton. Despite inaccurate ordering of the bright and dark excitons, the AM1 method gives a

sufficient qualitative dependence of the excitation energy on the tube diameter, slightly failing only for the tubes with diameters exceeding 1 nm. Substitution of the AM1 Hamiltonian with the semi-empirical ZINDO model leads to the appearance of the dark exciton below the bright one, see Table 1. However, in contrast to TD-DFT calculations, ZINDO yields the bright exciton as the second one after the lowest dark exciton for all tubes except the very narrow (6,2) and (8,0) chiralities. The splitting between these two excitons is notably smaller than those obtained with hybrid functionals. Particularly for long (6,5) and (8,6) tubes, dark and bright states are nearly degenerate. Compared to the other methods used here, the absolute values of excitation energies obtained using the ZINDO model are closer to the experimental ones (with a maximum deviation of ±0.1 eV for tubes with diameter exceeding 0.8 nm). Unfortunately, the dependence on the tube diameter is not satisfactory in the ZINDO case, even qualitatively.

The common concern with ZINDO is that it lacks a consistent parameterization. Particularly, it includes two fitting parameters that renormalize the Hamiltonian matrix elements and can be roughly related to the softness of π- and σ-bonds. These parameters are 1.267 and 0.585 in the ZINDO/S parameterization commonly used for spectroscopic property computations, respectively. To rationalize various results for the excitonic structure in SWNTs previously obtained with various theoretical methodologies[23–25,28,33,34,39,40,42] and in this work, we artificially varied the ZINDO/S parameters and observed the following emerging trends.

Fig. 5 demonstrates the dependence of excitation energies of the lowest dark and bright excitons on ZINDO parameters in SWNTs. Keeping one of the bond parameters as it is defined in ZINDO, the parameter of the other bond was varied. The larger the parameter, the more rigid and localized the bond appears, which is also related to the increase of long-range Coulombic interaction. Thus, approaching the π-bond parameter value of 1, (*i.e.*, making this bond more rigid), leads to a significant blue shift of excitation energies and simultaneously increases the bright–dark exciton splitting. In contrast, decreasing the π-bond parameter to 0.5 eV leads to red shifts and nearly degenerate bright and dark exciton states. Similar to the dependence on the π-bond parameter, increasing the softness of σ-bonds leads to a decrease of the bright–dark exciton splitting. Decrease of σ-bond to 1 results in the switching of the ordering between the bright and the dark excitons: the bright state becomes the lowest in energy, similar to the results obtained with the AM1 approach (insert in Fig. 5b). However, the excitation energies are shifted to the blue for small σ-bond parameter values, while increasing the σ-bond parameter leads to a red shift, compared to experimental values of the E_{11} transition. The tube length insignificantly affects the dependence of the bright–dark exciton splitting on the π-bond parameter. Thus, increase of the length results in a slight red-shift of the excitation energies and a small decrease in the splitting (Fig. 5b). Importantly, the dependence of the dark–bright exciton splitting on the π- and σ-bond parameters varies slightly with the tube chirality (Fig. 5a). This indicates that the same parameter might not work equally well for different tubes and explains the failure of ZINDO to accurately reproduce the diameter dependence of the excitation energies.

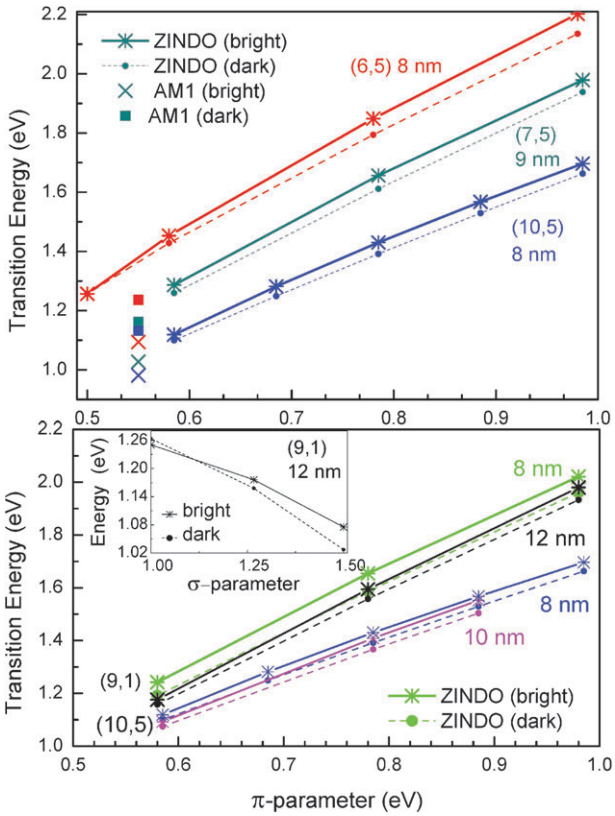

Fig. 5 Variation of the transition energy of the first dark and bright excitons in different tubes calculated with semi-empirical AM1 and ZINDO methods as a function of underlying parameters: (a) dependence of energies of dark (circles and dashed lines) and bright (stars and solid lines) excitons on ZINDO parameters characterizing the softness of π-bonds; (b) same as in panel (a) but comparing tubes of different length. The inset shows the dependence of excitation energies on the parameters characterizing the softness of σ-bonds.

4. Conclusions

We have reported computational results for excitonic structure in ten finite-size SWNTs obtained using TD-DFT and semiempirical TD-HF methods. We found that pure DFT functionals strongly delocalize electronic excitations, giving almost unbound electron–hole states; consequently, these functionals cannot be used for studies of excitonic effects in SWNTs. Correlated methods such as GWA and BSE built on top of the pure DFT overcome this problem.[25,58] Unfortunately, it is not currently feasible to apply this computationally intensive approach to a wide range of nanotube sizes. On the other hand, our calculations show that the pure TD-HF, while having only a moderate numerical expense, overbinds excitons because it does not account for dielectric screening effects related to the higher order electronic correlations. In particular, this method incorrectly predicts the lowest energy state to be the bright exciton.

In between these two limiting cases—0% (pure DFT functionals) and 100% (HF) of the long-range HF-exchange

contribution—there is a family of hybrid density functionals with varying portion of the HF-exchange fraction parametrically accounting for the dielectric screening effects. For example, the B3LYP (20%) model accurately describes electronic spectra in a variety of molecular systems. We found that this model provides the most accurate description of excitons and their energy splitting in SWNTs. Similar to conjugated polymers, increase of the HF-exchange in the functional (BHandHLYP, 50%) leads to substantial blue shifts of excitonic energies and a strong exciton localization, *i.e.*, a smaller particle–hole separation. Yet, the relative ordering and the energy splitting between the lowest dark and bright excitons, and the qualitative behavior of the excitation energy dependence on the tube diameter, are almost independent of the hybrid functional.

Thus, our TD-DFT calculations based on hybrid functionals unambiguously indicate that there are four important exciton bands (I–IV) related to the E_{11} transition, which is consistent with previous reports on finite-length SWNTs.[24,33] The lowest state is dark, the upper transition is bright (the first peak in the linear absorption spectra) and two semi-dark and nearly degenerate excitons lie in between. Because of the tube chirality and finite length of the considered tubes, sub-band states with the nodal structure in their transition density matrices appear weak in the spectra, which is consistent with experimental data.[28] The energy and oscillator strength of these states are found to be very sensitive to the functional used and on the tube length and chirality. In particular, decreasing the portion of the HF-exchange in the functional lowers energies of the sub-band states with respect to the bright exciton, while the splitting between the fundamental dark and bright excitons remains unchanged. The more delocalized character of the sub-band excitons allows mixing between neighboring excitons, including the bright one, making some of the sub-band states weakly optically active rather than strictly dark.

As expected, an increase of the tube length leads to a small red shift of excitation energies and a decrease of the bright–dark exciton splitting, as can be explained by small confinement effects introduced by the finite-length of the tubes we considered. For the short tubes with length smaller than 10 nm, semi-dark sub-band states noticeably contribute to the first absorption peak resulting in a larger broadening of absorption spectra. Importantly, the qualitative picture, including the relative position of dark I, semi-dark II–III, and bright IV excitons, and the overall structure of absorption spectra, are not changed for tubes with length exceeding 10 nm, *i.e.*, when the length of the tube is much larger than the exciton size. The calculated splitting between energies of the bright IV and dark I excitons in tubes longer than 10 nm is about 0.1 eV, showing weak dependence on the tube chirality. Although the obtained splitting is much larger than those calculated for infinite-length tubes,[23,25,34] this splitting could be further reduced with increase of the tube length.

Finally, we compared results of the first principles TD-DFT calculations with semi-empirical TD-HF methods. Similar to the *ab initio* TD-HF approach, the TD-HF method coupled with the AM1 Hamiltonian places the bright exciton below the dark one, which does not correlate with the results of recent time-resolved experiments and TD-DFT results. However, the dependence of the excitation energies on the tube diameter agrees well with experimental data, showing a consistent small red shift. The TD-HF method and the ZINDO Hamiltonian lead to changes in the exciton ordering, so that the lowest energy exciton is the dark one, followed by the bright exciton with a very small energy splitting ($\sim$0.3 eV for most tubes). However, the ZINDO model does not provide an accurate dependence of excitation energies on the tube diameter, even qualitatively. This discrepancy is likely to originate from the lack of a consistent parameterization in this Hamiltonian. Our analysis of trends in excitation energies appearing when varying ZINDO parameters allows us to link subtle interplays of the energetics of dark and bright excitons with the softness of chemical bonds and electronic delocalizations, which are accounted for differently in various theoretical methodologies used for modeling the electronic structure of SWNTs.

The detailed analysis we have presented and the comparison of first principle and semi-empirical methods based on linear response theory allows us to conclude that TD-DFT with functionals incorporating a small portion of HF-exchange, such as the B3LYP model, has the most generality and predictive capacity, providing the most reasonable and accurate description of excitonic structure in finite-size SWNTs.

Acknowledgements

This work was supported by the US Department of Energy and Los Alamos LDRD funds. Los Alamos National Laboratory is operated by Los Alamos National Security, LLC, for the National Nuclear Security Administration of the US Department of Energy under contract DE-AC52-06NA25396. We acknowledge the support of Center for Integrated Nanotechnology (CINT) and Center for Nonlinear Studies (CNLS).

References

1 M. J. Biercuk, N. Mason and C. M. Marcus, *Nano Lett.*, 2004, **4**, 1–4.
2 M. S. Dresselhaus, *Nature*, 2004, **432**, 959–960.
3 K. Terabe, T. Hasegawa, T. Nakayama and M. Aono, *Nature*, 2005, **433**, 47–50.
4 H. W. C. Postma, T. Teepen, Z. Yao, M. Grifoni and C. Dekker, *Science*, 2001, **293**, 76–79.
5 Z. H. Chen, J. Appenzeller, Y. M. Lin, J. Sippel-Oakley, A. G. Rinzler, J. Y. Tang, S. J. Wind, P. M. Solomon and P. Avouris, *Science*, 2006, **311**, 1735–1735.
6 B. F. Habenicht and O. V. Prezhdo, *Nature Nanotech.*, 2008, **3**, 190–191.
7 P. Avouris, Z. H. Chen and V. Perebeinos, *Nature Nanotech.*, 2007, **2**, 605–615.
8 Y. C. Chen, N. R. Raravikar, L. S. Schadler, P. M. Ajayan, Y. P. Zhao, T. M. Lu, G. C. Wang and X. C. Zhang, *Appl. Phys. Lett.*, 2002, **81**, 975–977.
9 S. Y. Set, H. Yaguchi, Y. Tanaka and M. Jablonski, *J. Lightwave Technol.*, 2004, **22**, 51–56.
10 S. Y. Set, H. Yaguchi, Y. Tanaka and M. Jablonski, *IEEE J. Sel. Top. Quantum Electron.*, 2004, **10**, 137–46.
11 J. A. Misewich, R. Martel, P. Avouris, J. C. Tsang, S. Heinze and J. Tersoff, *Science*, 2003, **300**, 783–786.
12 N. W. S. Kam, M. O'Connell, J. A. Wisdom and H. J. Dai, *Proc. Natl. Acad. Sci. U. S. A.*, 2005, **102**, 11600–11605.
13 C. L. Kane and E. J. Mele, *Phys. Rev. Lett.*, 2004, **93**, 197402.

14 C. D. Spataru, S. Ismail-Beigi, L. X. Benedict and S. G. Louie, *Phys. Rev. Lett.*, 2004, **92**, 774021.
15 A. Ruini, M. J. Caldas, G. Bussi and E. Molinari, *Phys. Rev. Lett.*, 2002, **88**, 206403–4.
16 Y. -Z. Ma, L. Valkunas, S. L. Dexheimer, S. M. Bachilo and G. R. Fleming, *Phys. Rev. Lett.*, 2005, **94**, 157402.
17 O. J. Korovyanko, C. X. Sheng, Z. V. Vardeny, A. B. Dalton and R. H. Baughman, *Phys. Rev. Lett.*, 2004, **92**, 017403.
18 A. Gambetta, C. Manzoni, E. Menna, M. Meneghetti, G. Cerullo, G. Lanzani, S. Tretiak, A. Piryatinski, A. Saxena, R. L. Martin and A. R. Bishop, *Nature Phys.*, 2006, **2**, 515–520.
19 F. Wang, G. Dukovic, L. E. Brus and T. F. Heinz, *Science*, 2005, **308**, 838–841.
20 P. M. Rafailov, J. Maultzsch, C. Thomsen and H. Kataura, *Phys. Rev. B*, 2005, **72**, 045411.
21 J. Maultzsch, R. Pomraenke, S. Reich, E. Chang, D. Prezzi, A. Ruini, E. Molinari, M. S. Strano, C. Thomsen and C. Lienau, *Phys. Rev. B*, 2005, **72**, 241402.
22 S. Uryu and T. Ando, *Phys. Rev. B*, 2006, **74**, 155411.
23 V. Perebeinos, J. Tersoff and P. Avouris, *Nano Lett.*, 2005, **74**, 2495–2499.
24 H. B. Zhao and S. Mazumdar, *Phys. Rev. Lett.*, 2004, **93**, 157402.
25 C. D. Spataru, S. Ismail-Beigi, R. B. Capaz and S. G. Louie, *Phys. Rev. Lett.*, 2005, **95**, 247402–4.
26 B. F. Habenicht and O. V. Prezhdo, *Phys. Rev. Lett.*, 2008, **100**, 197402–1.
27 B. F. Habenicht, C. F. Craig and O. V. Prezhdo, *Phys. Rev. Lett.*, 2006, **96**, 187401.
28 G. D. Scholes, S. Tretiak, T. J. McDonald, W. K. Metzger, C. Engtrakul, G. Rumbles and M. J. Heben, *J. Phys. Chem. C*, 2007, **111**, 11139–11149.
29 J. L. Blackburn, T. J. McDonald, W. K. Metzger, C. Engtrakul, G. Rumbles and M. J. Heben, *Nano Lett.*, 2008, **8**, 1047–1054.
30 A. Srivastava, H. Htoon, V. I. Klimov and J. Kono, *Phys. Rev. Lett.*, 2008, **1**(8), 01087402.
31 I. B. Mortimer and R. J. Nicholas, *Phys. Rev. Lett.*, 2007, **98**(2).
32 H. Kishida, Y. Nagasawa, S. Imamura and A. Nakamura, *Phys. Rev. Lett.*, 2008, **100**(9).
33 H. Zhao, S. Mazumdar, C. X. Sheng, M. Tong and Z. V. Vardeny, *Phys. Rev. B*, 2006, **73**, 75403.
34 R. B. Capaz, C. D. Spataru, S. Ismail-Beigi and S. G. Louie, *Phys. Rev. B*, 2006, **74**, 121401–1.
35 J. Shaver, J. Kono, O. Portugall, V. Krstic, G. Rikken, Y. Miyauchi, S. Maruyama and V. Perebeinos, *Nano Lett.*, 2007, **7**, 1851–1855.
36 Z. Zhu, J. Crochet, M. S. Arnold, M. C. Hersam, H. Ulbricht, D. Resasco and T. Hertel, *J. Phys. Chem. C*, 2007, **111**, 3831–3835.
37 Y. Z. Ma, L. Valkunas, S. M. Bachilo and G. R. Fleming, *Phys. Chem. Chem. Phys.*, 2006, **8**, 5689–5693.
38 M. Jones, W. K. Metzger, T. J. McDonald, C. Engtrakul, R. J. Ellingson, G. Rumbles and M. J. Heben, *Nano Lett.*, 2007, **7**, 300–306.
39 S. Kilina and S. Tretiak, *Adv. Funct. Mater.*, 2007, **17**, 3405–3420.
40 S. Kilina, S. Tretiak, S. K. Doorn, Z. Luo, F. Papadimitrakopoulos, A. Piryatinski, A. Saxena and A. R. Bishop, *Proc. Natl. Acad. Sci. U. S. A.*, 2008, **105**, 6797–6802.
41 Y. -Z. Ma, C. D. Spataru, L. Valkunas, S. G. Louie and G. R. Fleming, *Phys. Rev. B*, 2006, **74**, 085402.
42 S. Tretiak, *Nano Lett.*, 2007, **7**, 2201–2206.
43 S. Tretiak, S. Kilina, A. Piryatinski, A. Saxena, R. L. Martin and A. R. Bishop, *Nano Lett.*, 2007, **7**, 86–92.
44 J. L. Brédas, J. Cornil, D. Beljonne, D. A. dos Santos and Z. Shuai, *Acc. Chem. Res.*, 1999, **32**, 267–276.
45 S. Tretiak, A. Saxena, R. L. Martin and A. R. Bishop, *Phys. Rev. Lett.*, 2002, **89**, 097402.
46 S. Tretiak and S. Mukamel, *Chem. Rev.*, 2002, **102**, 3171–3212.
47 D. A. Heller, R. M. Mayrhofer, S. Baik, Y. V. Grinkova, M. L. Usrey and M. S. Strano, *J. Am. Chem. Soc.*, 2004, **126**, 14567–14573.
48 D. Yarotski, S. Kilina, A. Talin, S. Tretiak, A. Balatsky and A. Taylor, *Nano Lett.*, 2009, in press.
49 M. J. S. Dewar, E. G. Zoebisch, E. F. Healy and J. J. P. Stewart, *J. Am. Chem. Soc.*, 1985, **107**, 3902–3909.
50 J. J. P. Stewart, *MOPAC 2002*, Schrödinger Inc. and Fujitsu Limited, Portland, OR 97201, 2000.
51 P. T. Araujo, S. K. Doorn, S. Kilina, S. Tretiak, E. Einarsson, S. Maruyama, H. Chacham, M. A. Pimenta and A. Jorio, *Phys. Rev. Lett.*, 2007, **98**, 067401.
52 A. P. Shreve, E. H. Haroz, S. M. Bachilo, R. B. Weisman, S. Tretiak, S. Kilina and S. K. Doorn, *Phys. Rev. Lett.*, 2007, **98**, 037405.
53 M. J. Frisch, G. W. Trucks, H. B. Schlegel, G. E. Scuseria, M. A. Robb, J. R. Cheeseman, J. A. Montgomery, Jr, T. Vreven, K. N. Kudin, J. C. Burant, J. M. Millam, S. S. Iyengar, J. Tomasi, V. Barone, B. Mennucci, M. Cossi, G. Scalmani, N. Rega, G. A. Petersson, H. Nakatsuji, M. Hada, M. Ehara, K. Toyota, R. Fukuda, J. Hasegawa, M. Ishida, T. Nakajima, Y. Honda, O. Kitao, H. Nakai, M. Klene, X. Li, J. E. Knox, H. P. Hratchian, J. B. Cross, V. Bakken, C. Adamo, J. Jaramillo, R. Gomperts, R. E. Stratmann, O. Yazyev, A. J. Austin, R. Cammi, C. Pomelli, J. W. Ochterski, P. Y. Ayala, K. Morokuma, G. A. Voth, P. Salvador, J. J. Dannenberg,V. G. Zakrzewski, S. Dapprich, A. D. Daniels, M. C. Strain, O. Farkas, D. K. Malick, A. D. Rabuck, K. Raghavachari, J. B. Foresman, J. V. Ortiz, Q. Cui, A. G. Baboul, S. Clifford, J. Cioslowski, B. B. Stefanov, G. Liu, A. Liashenko, P. Piskorz, I. Komaromi, R. L. Martin, D. J. Fox, M. A. A.-L. T. Keith, C. Y. Peng, A. Nanayakkara, M. Challacombe and P. M. W., *GAUSSIAN Dev. Ver. (Rev. D.02)*, Gaussian, Inc., Wallingford, CT, 2004.
54 S. Tretiak, K. Igumenshchev and V. Chernyak, *Phys. Rev. B*, 2005, **71**, 33201.
55 C. Wu, S. V. Malinin, S. Tretiak and V. Y. Chernyak, *Nature Phys.*, 2006, **2**, 631–635.
56 Z. G. Yu, D. L. Smith, A. Saxena, R. L. Martin and A. R. Bishop, *Phys. Rev. Lett.*, 2000, **84**, 721–4.
57 R. B. Weisman and S. M. Bachilo, *Nano Lett.*, 2003, **3**, 1235–1238.
58 E. Chang, G. Bussi, A. Ruini and E. Molinari, *Phys. Rev. Lett.*, 2004, **92**, 196401.